Inorg. Chem. **2003**, *42*, 2357−2361

A Vanadium(IV) Phosphite with a Pillared Layered Structure: Hydrothermal Synthesis and Characterization of $(VO)_4(4,4'\text{-bpy})_2(HPO_3)_4$

Zhan Shi, Guanghua Li, Dong Zhang, Jia Hua, and Shouhua Feng*

State Key Laboratory of Inorganic Synthesis and Preparative Chemistry, College of Chemistry, Jilin University, Changchun 130023, P. R. China

Received November 9, 2002

A novel vanadium(IV) phosphite, $(VO)_4(4,4'\text{-bpy})_2(HPO_3)_4$, was hydrothermally synthesized and characterized by single-crystal X-ray diffraction. This compound crystallizes in the monoclinic system with the space group *C*2/*c* and cell parameters $a = 35.970(3)$ Å, $b = 15.9400(13)$ Å, $c = 10.7681(7)$ Å, $\beta = 101.073(4)°$, and $Z = 8$ with $R_1 = 0.0482$. The structure of the compound consists of trigonal bipyramidal [VO_4N] and pseudopyramidal [HPO_3] blocks, which are connected by corner-sharing, to form vanadium phosphite layers in the *bc* plane. These layers are further linked through 4,4′-bpy pillars, generating a 3D framework. Thermogravimetric analysis and magnetic susceptibility data for this compound are given.

Introduction

The design and synthesis of inorganic−organic hybrid materials have provoked significant interests owing to their rich structural chemistry and potential applications in catalysis, biology, and optical and electromagnetic functions.[1−4] Huge structures of these materials were reported, showing various architectures with one- (1D), two- (2D), and three-dimensional (3D) connections between inorganic and organic species.[5−7] A study of the literature of inorganic−organic hybrid materials showed that 4,4′-bpy molecule was the most extensively used organic ligand to achieve various open framework structures, for its strong coordination ability and its own size and shape. The 4,4′-bpy molecule may serve several functions in the inorganic−organic hybrid materials including (1) as an organic template and charge-compensating cation, such as in $(4,4'\text{-}H_2bpy)(Mo_7O_{22})\cdot H_2O$,[8] (2) as a pillar directly bonding to inorganic skeletal backbone, such as in $Zn_2(4,4'\text{-bpy})(PO_3F)_2$,[9] and (3) as a ligand linking both a metal and an inorganic framework, such as in $[Cu(4,4'\text{-bpy})](VO_2)(PO_4)$.[10] Other interesting compounds in metal/phosphate/4,4′-bpy systems are $[Ga_4(4,4'\text{-Hbpy})_2(PO_4)(H_{0.5}PO_4)_2(HPO_4)_2(H_2PO_4)_2(H_2O)_2]\cdot H_2O$ (1D),[11] $[Ni(4,4'\text{-bpy})_2(H_2PO_4)_2]\cdot C_4H_9OH\cdot H_2O$ (2D),[12] and $[In_4(4,4'\text{-bpy})_3(HPO_4)_4(H_2PO_4)_4]_4\cdot H_2O$ (3D)[13] and others, especially three interesting vanadium/phosphate/4,4′-bpy compounds $(4,4'\text{-}H_2bpy)[V_2(HPO_4)_4(4,4'\text{-bpy})_2]$ (2D),[14] $[(VO_2)_2(4,4'\text{-bpy})_{0.5}(4,4'\text{-Hbpy})(PO_4)]\cdot H_2O$ (2D),[15] and $(NH_4)[(V_2O_3)_2(4,4'\text{-bpy})_2(H_2PO_4)(PO_4)_2]\cdot 0.5H_2O$ (3D).[16] Moreover, the replacement of phosphate by phosphite in these systems has been taken account, since the incorporation of the pseudopyramidal hydrogen phosphite group $[HPO_3]^{2-}$ created

* To whom correspondence should be addressed. E-mail: shfeng@mail.jlu.edu.cn. Fax: +86-431-5671974. Tel: +86-431-5670650.

(1) Ferey, G. *Chem. Mater.* **2001**, *13*, 3084−3098 and references therein.
(2) Hagrman, P. J.; Hagrman, D.; Zubieta, J. *Angew. Chem., Int. Ed.* **1999**, *38*, 2638−2684 and references therein.
(3) Cheetham, A. K.; Ferey, G.; Loiseau, T. *Angew. Chem., Int. Ed.* **1999**, *38*, 3268−3292 and references therein.
(4) Eddaoudi, M.; Moler, D. B.; Li, H.; Chen, B.; Reineke, T. M.; O′keeffe, M.; Yaghi, O. M. *Acc. Chem. Res.* **2001**, *34*, 319−330.
(5) Shi, Z.; Feng, S.; Gao, S.; Zhang, L.; Yang, G.; Hua, J. *Angew. Chem., Int. Ed.* **2000**, *39*, 2325−2327.
(6) Shi, Z.; Zhang, D.; Feng, S.; Li, G.; Dai, Z.; Fu, W.; Chen, X.; Hua, J. *J. Chem. Soc., Dalton Trans.* **2002**, 1873−1874.
(7) Shi, Z.; Zhang, L.; Zhu, G.; Yang, G.; Hua, J.; Ding, H.; Feng, S. *Chem. Mater.* **1999**, *11*, 3565−3570.
(8) Zapf, P. J.; Haushalter, R. C.; Zubieta, J. *Chem. Commun.* **1997**, 321−322.
(9) Halasyamani, P. S.; Drewitt, M. J.; O′Hare, D. *Chem. Commun.* **1997**, 867−868.
(10) Shi, Z.; Feng, S.; Zhang, L.; Yang, G.; Hua, J. *Chem. Mater.* **2000**, *12*, 2930−2935.
(11) Chen, C. Y.; Lo, F. R.; Kao, H. M.; Lii, K. H. *Chem. Commun.* **2000**, 1061−1062.
(12) Jiang, Y. C.; Lai, Y. C.; Wang, S. L.; Lii, K. H. *Inorg. Chem.* **2001**, *40*, 5320−5321.
(13) Lii, K. H.; Huang, Y. F. *Inorg. Chem.* **1999**, *38*, 1348−1350.
(14) Huang, C. H.; Huang, L. H.; Lii, K. H. *Inorg. Chem.* **2001**, *40*, 2625−2627.
(15) Huang, L. H.; Kao, H. M.; Lii, K. H. *Inorg. Chem.* **2002**, *41*, 2936−2940.
(16) Hung, L. I.; Wang, S. L.; Kao, H. M.; Lii, K. H. *Inorg. Chem.* **2002**, *41*, 3929−3934.

10.1021/ic0261676 CCC: $25.00
Published on Web 03/06/2003

several novel structures, such as organically templated cobalt phosphite,[17] manganese phosphites,[18,19] zinc phosphites,[20−25] and vanadium phosphites.[26]

Our group has developed the hydrothermal synthesis of inorganic−organic metal phosphites and found novel compounds $[H_3NCH_2CH(NH_3)CH_3]\cdot[Zn_2(HPO_3)_3]\cdot H_2O$, $[H_3N(CH_2)_6NH_3]\cdot[Zn_3(HPO_3)_4]$, $[HN(C_2H_4)_3N][(VO)_2(OH)(H_2O)(HPO_3)_2]\cdot H_2O$, etc.[27,28] All reported inorganic−organic hybrid phosphites have exhibited distinguished structural features due to the particular geometry of the building block of phosphite and the lower oxidation states of phosphorus atom. The oxidation states of phosphorus atoms may directly influence the reactivity of secondary coordination oxygen atoms with for example adjacent metals. In this paper, we report a new compound $(VO)_4(4,4'\text{-bpy})_2(HPO_3)_4$, **1**, which consists of layers of vanadium(IV) phosphite pillared through 4,4′-bpy ligands into a 3D structure. It is the first example for the hybrid compound prepared in the vanadium/phosphite/4,4′-bpy system. The magnetic susceptibility and thermogravimetric data are also reported.

Experimental Section

Synthesis and Characterization. The title compound was prepared from a reaction mixture of vanadium oxide (V_2O_5), phosphorous acid (H_3PO_3), 4,4′-bipyridine (4,4′-bpy·$2H_2O$), tetramethylammonium hydroxide pentahydrate ((TMA)OH·$5H_2O$), and distilled water with a molar ratio of 1.0:10.0:2.0:8.0:555 V_2O_5:H_3PO_3:4,4′-bpy:(TMA)OH·H_2O:H_2O. A typical procedure began with mixing 0.091 g of V_2O_5, 0.410 g of H_3PO_3, 0.725 g of (TMA)OH·H_2O, and 0.192 g of 4,4′-bpy·$2H_2O$ with 5 mL of H_2O to form a reaction mixture. The role of (TMA)OH is to regulate the pH value of the system. The mixture was heated in a sealed Teflon-lined steel autoclave at 160 °C for 120 h. The resulting green crystals were washed with distilled water, filtered off, and dried in air. The yield of product was 72% in weight based on vanadium.

The elemental analysis was conducted on a Perkin-Elmer 2400 elemental analyzer. Inductively coupled plasma (ICP) analysis was performed on a Perkin-Elmer Optima 3300DV ICP instrument. ICP analysis for the product gave the contents of V 22.36 wt % (calcd 22.64 wt %) and P 13.86% (calcd 13.77 wt %), indicating a V:P ratio of 1:1. Elemental analysis showed that the sample contains 26.80, 1.86, and 6.15 wt % of C, H, and N, respectively, in agreement with the expected values of 26.69, 1.78, and 6.22 wt % of C, H, and N on the basis of the empirical formula given by the single-crystal structure analysis.

X-ray powder diffraction (XRD) data were collected on a Siemens D5005 diffractometer with Cu Kα radiation ($\lambda = 1.5418$ Å). The step size was 0.02°, and the count time was 4 s. The infrared (IR) spectrum was recorded within the 400−4000 cm^{-1} region on a Nicolet Impact 410 FTIR spectrometer using KBr pellets. A Perkin-Elmer DTA 1700 differential thermal analyzer was used to obtain the differential thermal analysis (DTA) and a Perkin-Elmer TGA 7 thermogravimetric analyzer to obtain thermogravimetric analysis (TGA) curves in an atmospheric environment with a heating rate of 10 °C min^{-1}.

Magnetic susceptibility data were collected on the basis of a 0.0603 g sample over the temperature range 2.4−300 K at a magnetic field of 5 kG on a Quantum Design MPMS-7 SQUID magnetometer.

Determination of Crystal Structure. A suitable green single crystal with dimensions 0.210 × 0.200 × 0.160 mm was glued to a thin glass fiber and mounted on a Siemens Smart CCD diffractometer equipped with a normal-focus, 2.4-kW sealed-tube X-ray source (graphite-monochromatic Mo Kα radiation ($\lambda = 1.5418$ Å) operating at 50 kV and 40 mA. Intensity data were collected at a temperature of 20 ± 2 °C. Date processing was accomplished with the SAINT processing program.[29] The total number of measured reflections and observed unique reflections were 14502 and 4340, respectively. Intensity data of 4340 independent reflections ($-39 \le h \le 39$, $-9 \le k \le 17$, $-11 \le l \le 11$) were collected in the ω scan mode. An empirical absorption correction was applied using the SADABS program with $T_{min} = 0.248$ and $T_{max} = 0.334$. The structure was solved in the space group $C2/c$ by direct methods and refined on F^2 by full-matrix least squares using SHELXTL97. The phosphorus and vanadium atoms were located first. Carbon, nitrogen, and oxygen were then found in the difference Fourier map. The hydrogen atoms that are bonded to carbon and nitrogen atoms were placed geometrically; the hydrogen atoms that are bonded to phosphorus atoms were located in the difference Fourier map. All non-hydrogen atoms were refined with anisotropic thermal parameters.

Results and Discussion

Characterization. Powder X-ray diffraction pattern for $(VO)_4(4,4'\text{-bpy})_2(HPO_3)_4$ was entirely consistent with the simulated one on the basis of the single-crystal structure,[30] as shown in Figure 1. The diffraction peaks on both patterns corresponded well in position, indicating the phase purity of the as-synthesized sample. The difference in reflection intensities between the simulated and experimental patterns was due to the variation in crystal orientation for the power sample.

Thermogravimetic analysis indicated the weight loss of the sample ca. 33.45% in the temperature range from 420 to 800 °C, corresponding to the decomposition of 4,4′-bpy molecular (calcd 34.65%). Accordingly, the DTA curve exhibited three exothermic peaks for the decomposition of the organic template in air. The structure was collapsed at 420 °C when the organic part was lost.

(17) Fernandez, S.; Pizarro, J. L.; Mesa, J. L.; Lezama, L.; Arriortua, M. I.; Rojo, T. *Int. J. Inorg. Mater.* **2001**, *3*, 331−336.
(18) Fernandez, S.; Pizarro, J. L.; Mesa, J. L.; Lezama, L.; Arriortua, M. I.; Olazcuaga, R.; Rojo, T. *Inorg. Chem.* **2001**, *40*, 3476−3483.
(19) Fernandez, S., Mesa, J. L., Pizarro, J. L., Lezama, L., Arriortua, M. I., Olazcuaga, R.; Rojo, T. *Chem. Mater.* **2000**, *12*, 2092−2098.
(20) Harrison, W. T. A. *Int. J. Inorg. Mater.* **2001**, *3*, 187−189.
(21) Rodgers, J. A.; Harrison, W. T. A. *Chem. Commun.* **2000**, 2385−2386.
(22) Harrison, W. T. A.; Phillips, M. L. F.; Stanchfield, J.; Nenoff, T. M. *Inorg. Chem.* **2001**, *40*, 895−899.
(23) Harrison, W. T. A. *J. Solid State Chem.* **2001**, *160*, 4−7.
(24) Harrison, W. T. A.; Phillips, M. L. F.; Nenoff, T. M. *J. Chem. Soc., Dalton Trans.* **2001**, 2459−2461.
(25) Harrison, W. T. A.; Phillips, M. L. F.; Nenoff, T. M. *Int. J. Inorg. Mater.* **2001**, *3*, 1033−1038.
(26) Bonavia, G.; DeBord, J.; Haushalter, R. C.; Rose, D.; Zubieta, J. *Chem. Mater.* **1995**, *7*, 1995−1998.
(27) Fu, W.; Shi, Z.; Zhang, D.; Li, G.; Dai, Z.; Chen, X.; Feng, S. *J. Solid State Chem.*, submitted for publication.
(28) Shi, Z.; Zhang, D.; Li, G.; Wang, L.; Lu, X.; Hua, J.; Feng, S. *J. Solid State Chem.* **2003**, in press.
(29) *Software Packages SMART and SAINT*; Siemens Analytical X-ray Instruments Inc.: Madison, WI, 1996. *SHELXTL*, version 5.1; Siemens Industrial Automation, Inc.: Madison, WI, 1997.
(30) *PowderCell for Windows*, version 2.4; Federal Institute for Materials Research and Testing: Berlin, 2000.

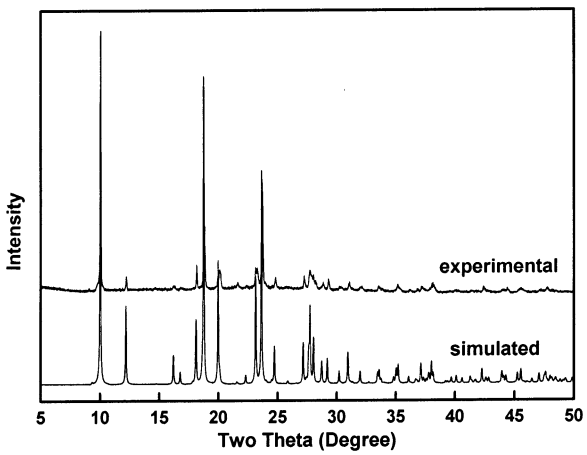

Figure 1. Experimental and simulated power X-ray diffraction patterns for $(VO)_4(4,4'\text{-bpy})_2(HPO_3)_4$.

Table 1. Crystallographic Data for $(VO)_4(4,4'\text{-bpy})_2(HPO_3)_4$

empirical formula	$C_{20}H_{20}N_4V_4P_4O_{16}$
fw	900.04
space group	*C*2/*c* (No. 15)
a, Å	35.970(3)
b, Å	15.9400(13)
c, Å	10.7681(7)
β, deg	101.073(4)
V, Å^3	6059.0(8)
Z	8
T, K	293(2)
λ(Mo Kα), Å	0.710 73
ρ_{calc}, g cm^{-3}	1.973
μ(Mo Kα), mm^{-1}	1.489
$R_1{}^a$ [$I > 2\sigma(I)$]	0.0482
$wR_2{}^b$ [$I > 2\sigma(I)$]	0.1560

^{a} $R_1 = \sum||F_o| - |F_c||/\sum|F_o|$. ^{b} $wR_2 = \{\sum[w(F_o^2 - F_c^2)^2]/\sum[w(F_o^2)]^2\}^{1/2}$, $w = 1/[\sigma^2|F_o|^2 + (0.0782P)^2 + 17.5877P]$, where $P = [\text{Max}|F_o|^2 + 2|F_c|^2]/3$.

IR spectrum of the sample showed that the stretching vibrations of C−H and N−H bands were from 3050 to 2900 cm^{-1}, and the bands at 1612, 1535, 1492, and 1417 cm^{-1} were associated with the pyridine ring stretching vibrations. The bands at 1138, 1063, 1023, and 995 cm^{-1} were associated with the stretching vibrations of V−O and P−O bonds, respectively. There appeared the absorptions at 2426 cm^{-1} due to the stretching vibrations of the H−P groups in phosphite anions.

Description of the Structure. The crystallographic data for **1** are given in Table 1. Selected bond distances and angles are listed in Table 2. An ORTEP drawing of the asymmetric unit of the structure is shown in Figure 2. It crystallizes in the monoclinic space group *C*2/*c* with a unit cell content of eight formula units. All atoms are at general positions. There are four unique vanadium ions, four unique phosphorus ions, and two 4,4′-bpy ligands in an asymmetric unit. The two ligands in the asymmetric unit as rodlike ligands have the same coordinative mode. Each of the 4,4′-bpy ligands bridges two vanadium sites to form a $\{V_2(4,4'\text{-bpy})\}$ fragment. However, one of them is nearly planar with the two pyridyl rings twisted by 6.9°. The another is not planar, and the two rings are twisted at an angle of 26.4°. In this structure, the independent vanadium atoms have the same coordination geometries. Each of the four vanadium sites in an asymmetric unit exhibits a distorted trigonal bipyramidal geometry with $[VO_4N]$, the basal positions defined by oxygen donors from two adjacent phosphite groups and a terminal oxide (the

Table 2. Selected Bond Lengths (Å) and Angles (deg) for $(VO)_4(4,4'\text{-bpy})_2(HPO_3)_4{}^{a,b}$

V(1)−O(1)	1.574(6)	V(2)−O(5)	1.586(6)
V(1)−O(2)	1.923(6)	V(2)−O(6)	1.980(5)
V(1)−O(3)	1.993(5)	V(2)−O(7)	1.931(6)
V(1)−O(4)	1.942(5)	V(2)−O(8)	1.938(5)
V(1)−N(1)	2.171(7)	V(2)−N(3)	2.146(6)
V(3)−O(9)	1.563(6)	V(4)−O(13)	1.569(6)
V(3)−O(10)	1.982(5)	V(4)−O(14)	1.983(5)
V(3)−O(11)	1.926(6)	V(4)−O(15)	1.932(6)
V(3)−O(12)	1.947(5)	V(4)−O(16)	1.932(5)
V(3)−N(2)$^{\#1}$	2.159(7)	V(4)−N(4)$^{\#2}$	2.158(7)
P(1)−O(4)	1.504(5)	P(2)−O(7)$^{\#4}$	1.492(6)
P(1)−O(6)	1.515(6)	P(2)−O(8)	1.521(5)
P(1)−O(11)$^{\#3}$	1.492(6)	P(2)−O(10)	1.519(6)
P(1)−H(1P)	1.33(9)	P(2)−H(2P)	1.37(9)
P(3)−O(2)$^{\#3}$	1.501(6)	P(4)−O(3)$^{\#6}$	1.522(6)
P(3)−O(12)	1.509(5)	P(4)−O(15)$^{\#5}$	1.497(6)
P(3)−O(14)	1.515(6)	P(4)−O(16)	1.532(5)
P(3)−H(3P)	1.36(9)	P(4)−H(4P)	1.44(8)
N(1)−C(1)	1.298(11)	N(3)−C(11)	1.333(11)
N(1)−C(5)	1.266(11)	N(3)−C(15)	1.357(9)
N(2)−C(6)	1.293(11)	N(4)−C(16)	1.339(10)
N(2)−C(10)	1.319(11)	N(4)−C(20)	1.332(11)
C(1)−C(2)	1.283(14)	C(11)−C(12)	1.387(12)
C(2)−C(3)	1.385(14)	C(12)−C(13)	1.382(11)
C(3)−C(4)	1.338(11)	C(13)−C(14)	1.372(12)
C(3)−C(8)	1.513(14)	C(13)−C(18)	1.463(13)
C(4)−C(5)	1.363(13)	C(14)−C(15)	1.399(11)
C(6)−C(7)	1.371(12)	C(16)−C(17)	1.408(11)
C(7)−C(8)	1.354(11)	C(17)−C(18)	1.352(12)
C(8)−C(9)	1.376(13)	C(18)−C(19)	1.385(11)
C(9)−C(10)	1.315(13)	C(19)−C(20)	1.374(12)
O(1)−V(1)−O(2)	113.2(3)	O(5)−V(2)−O(7)	113.1(3)
O(1)−V(1)−O(4)	117.2(3)	O(5)−V(2)−O(8)	116.2(3)
O(2)−V(1)−O(4)	129.1(3)	O(7)−V(2)−O(8)	129.9(3)
O(1)−V(1)−O(3)	101.2(3)	O(5)−V(2)−O(6)	101.2(3)
O(2)−V(1)−O(3)	89.7(2)	O(7)−V(2)−O(6)	89.9(2)
O(4)−V(1)−O(3)	87.8(2)	O(8)−V(2)−O(6)	88.9(2)
O(1)−V(1)−N(1)	95.0(3)	O(5)−V(2)−N(3)	95.5(3)
O(2)−V(1)−N(1)	84.4(2)	O(7)−V(2)−N(3)	83.5(2)
O(4)−V(1)−N(1)	84.3(2)	O(8)−V(2)−N(3)	83.6(2)
O(3)−V(1)−N(1)	163.8(3)	O(6)−V(2)−N(3)	163.3(3)
O(9)−V(3)−O(11)	112.2(3)	O(13)−V(4)−O(16)	117.0(3)
O(9)−V(3)−O(12)	115.5(3)	O(13)−V(4)−O(15)	112.1(3)
O(11)−V(3)−O(12)	131.7(3)	O(16)−V(4)−O(15)	130.2(3)
O(9)−V(3)−O(10)	101.4(3)	O(13)−V(4)−O(14)	101.5(3)
O(11)−V(3)−O(10)	89.8(2)	O(16)−V(4)−O(14)	88.4(2)
O(12)−V(3)−O(10)	88.4(2)	O(15)−V(4)−O(14)	89.7(2)
O(9)−V(3)−N(2)$^{\#1}$	95.3(3)	O(13)−V(4)−N(4)$^{\#2}$	94.3(3)
O(11)−V(3)−N(2)$^{\#1}$	84.2(3)	O(16)−V(4)−N(4)$^{\#2}$	83.9(2)
O(12)−V(3)−N(2)$^{\#1}$	84.1(2)	O(15)−V(4)−N(4)$^{\#2}$	84.9(2)
O(10)−V(3)−N(2)$^{\#1}$	163.3(3)	O(14)−V(4)−N(4)$^{\#2}$	164.2(3)
O(11)$^{\#3}$−P(1)−O(4)	110.0(4)	O(7)$^{\#4}$−P(2)−O(10)	114.5(3)
O(11)$^{\#3}$−P(1)−O(6)	113.8(4)	O(7)$^{\#4}$−P(2)−O(8)	109.6(4)
O(4)−P(1)−O(6)	110.7(3)	O(10)−P(2)−O(8)	110.0(3)
O(11)$^{\#3}$−P(1)−H(1P)	106(4)	O(7)$^{\#4}$−P(2)−H(2P)	106(4)
O(4)−P(1)−H(1P)	113(4)	O(10)−P(2)−H(2P)	108(4)
O(6)−P(1)−H(1P)	103(4)	O(8)−P(2)−H(2P)	109(3)
O(2)$^{\#3}$−P(3)−O(12)	110.0(3)	O(15)$^{\#5}$−P(4)−O(3)$^{\#6}$	114.5(3)
O(2)$^{\#3}$−P(3)−O(14)	113.8(3)	O(15)$^{\#5}$−P(4)−O(16)	110.4(3)
O(12)−P(3)−O(14)	110.5(3)	O(3)$^{\#6}$−P(4)−O(16)	109.8(3)
O(2)$^{\#3}$−P(3)−H(3P)	107(4)	O(15)$^{\#5}$−P(4)−H(4P)	101(3)
O(12)−P(3)−H(3P)	109(3)	O(3)$^{\#6}$−P(4)−H(4P)	114(4)
O(14)−P(3)−H(3P)	107(4)	O(16)−P(4)−H(4P)	107(3)
P(3)$^{\#4}$−O(2)−V(1)	148.7(4)	P(2)−O(10)−V(3)	134.5(3)
P(4)$^{\#7}$−O(3)−V(1)	133.9(3)	P(1)$^{\#4}$−O(11)−V(3)	149.1(4)
P(1)−O(4)−V(1)	136.9(4)	P(3)−O(12)−V(3)	137.4(4)
P(1)−O(6)−V(2)	134.4(4)	P(3)−O(14)−V(4)	136.2(4)
P(2)$^{\#3}$−O(7)−V(2)	148.4(4)	P(4)$^{\#8}$−O(15)−V(4)	146.8(4)
P(2)−O(8)−V(2)	137.0(3)	P(4)−O(16)−V(4)	136.3(3)

^{a} The C−H bond lengths are 0.93 Å. ^{b} #1, $-x + 1/2$, $-y + 1/2$, $-z - 1$; #2, $-x + 1$, $-y$, $-z + 1$; #3, x, $-y + 1$, $z + 1/2$; #4, x, $-y + 1$, $z - 1/2$; #5, x, $-y$, $z - 1/2$; #6, x, $y - 1$, z; #7, x, $y + 1$, z; #8, x, $-y$, $z + 1/2$.

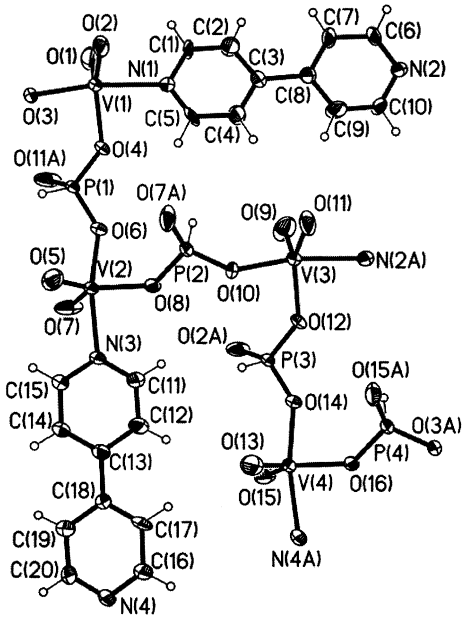

Figure 2. ORTEP view of the structure of $(VO)_4(4,4'\text{-bpy})_2(HPO_3)_4$, showing the atom-labeling scheme (50% thermal ellipsoids).

classical short-bond V═O, average $V-O_{av}$ 1.573 Å) and the apical positions by an oxygen donor from another adjacent phosphite group and one nitrogen atom of a 4,4′-bpy molecule. Bond-length and bond-strength calculations were based on the method and data from Brown, Shannon, and Altermatt.[31,32] The bond valence sums (BVS) calculations assuming V(1)−V(4) bonds gave the values of 3.67, 3.63, 3.73, and 3.71, respectively, indicating all V atoms are tetravalent. The magnetic measurement supported the BVS calculations. All of the four phosphite groups in an asymmetric unit adopt the same μ_3-coordination mode, different from the μ_4-coordination for the phosphates. The P atom has its three oxygen atoms bonded to three V atoms. The HPO_3 exhibits similar P−O bond distances, with a mean value of 1.51 Å. The H−P bond distances are similar in all phosphite anions. The O−P−O angles are in the range from 109.6(4) to 114.5(3)°, while the H−P−O angles range from 103(4) to 109(3)°.

The structure of **1** consists of $[VO_4N]$ trigonal bipyramids that are connected by corner-sharing pseudopyramidal units $[HPO_3]^{2-}$ to form layers in the *bc*-plane (Figure 3), which are further linked through 4,4′-bpy pillars to generate a 3D open framework (Figures 4 and 5).

A view of the structure perpendicular to the plane of the V/P/O layer orientated in the [100] plane is shown in Figure 3. The infinite neutral layers $[(VON)(HPO_3)]_\infty$ are composed of corner-sharing trigonal bipyramidal $[VO_4N]$ and pseudopyramidal $[HPO_3]$ units fused together via V−O−P bonds. First, each $[VO_4N]$ group forms two V−O−P links, resulting in polyhedral $[(VO_4N)(HPO_3)]_2$ four-membered rings with strict alternation of the V and P species. Two of the V−N bonds in one $[(VO_4N)(HPO_3)]_2$ four-membered ring project from alternate sides in an ordered fashion. Then, the

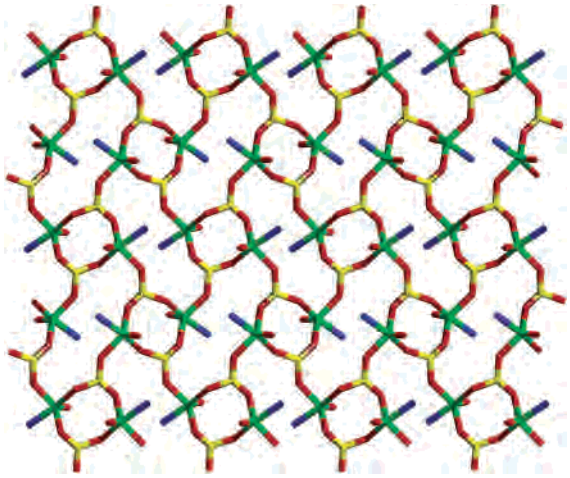

Figure 3. View of the V/P/O layer of $(VO)_4(4,4'\text{-bpy})_2(HPO_3)_4$. Color code: V atoms, green; P atoms, yellow; N atoms, blue; O atoms, red.

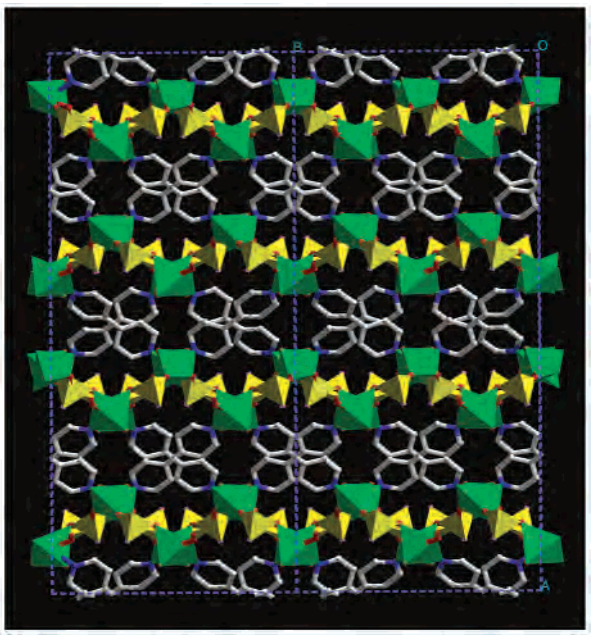

Figure 4. View of the structure of $(VO)_4(4,4'\text{-bpy})_2(HPO_3)_4$, along the *c*-axis. Color code: the VO_4N trigonal bipyramid, green, the HPO_3 pseudopyramid, yellow; C atoms, white; N atoms, blue; O atoms, red; H atoms of the HPO_3 pseudopyramid, purple.

remaining oxygens of the $[(VO_4N)(HPO_3)]_2$ four-membered rings link other four-membered rings, forming eight-membered rings. The distances between the two opposite vanadium atoms in the eight-membered rings are 5.194 and 10.398 Å. Thus, a 4.8-membered ring network of a $[(VON)(HPO_3)]_\infty$ layer was formed. It is noteworthy that, unlike other layered vanadium phosphates or vanadium phosphites, this layer is the folded layer along the *c*-axes, as seen in Figure 4.

The adjacent V/P/O layers are connected by 4,4′-bpy ligands, generating a 3D structure. The bridged V···V distance along 4,4′-bpy is ca. 11.4 Å. The close contact distance between adjacent 4,4′-bpy ligands is 3.65 Å. The size of this channel is a direct consequence of the V−4,4′-bpy−V linkage (Figure 5). The 4,4′-bpy ligands increase the

(31) Brown, I. D.; Shannon, R. D. *Acta Crystallogr.* **1973**, *A29*, 266−282.
(32) Brown, I. D.; Altermatt, D. *Acta Crystallogr.* **1985**, *B41*, 244−247.

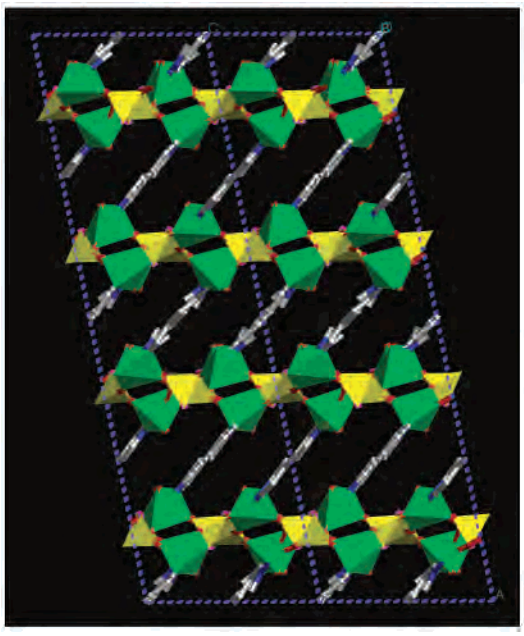

Figure 5. View of the structure of (VO)$_4$(4,4′-bpy)$_2$(HPO$_3$)$_4$, along the *b*-axis. Color code: the VO$_4$N trigonal bipyramid, green, the HPO$_3$ pseudopyramid, yellow; C atoms, white; N atoms, blue; O atoms, red; H atoms of the HPO$_3$ pseudopyramid, purple.

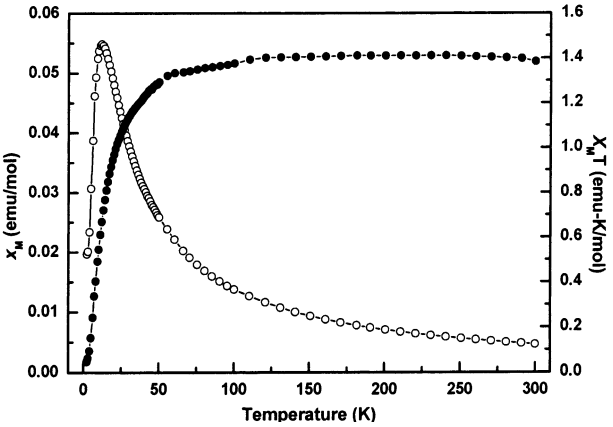

Figure 6. Thermal evolution of χ_m (○) and $\chi_m T$ (●) curves of (VO)$_4$(4,4′-bpy)$_2$(HPO$_3$)$_4$.

distance between the vanadium ions, producing the observed channel and extending the 2D V/P/O layers into a 3D structure.

Magnetic Susceptibility. Magnetic susceptibility plots of χ_m and $\chi_m T$ vs T for **1** are showed in Figure 6 over the temperature range 2.4−300 K. The measured data were fitted using the Curie−Weiss equation $\chi_m = C_m/(T - \Theta)$ at temperatures >50 K, where χ_m is the measured magnetic susceptibility, T the temperature (K), C_m the Curie constant, and Θ the Weiss constant, with $C_m = 1.422$ emu K^{-1} mol^{-1} and $\Theta = -2.996$ K, exhibiting a maximum in χ_m at 12 K. This result together with the decrease in the $\chi_m T$ values below 100 K is indicative of antiferromagnetic interaction in the compound. At 300 K, the calculated effective magnetic moment/vanadium atom, determined from the equation $\mu_{eff} = 2.828(1.384/4)^{1/2}$, is 1.66 μ_B, in good agreement with the predicted spin-only value of 1.73 μ_B for a d^1 vanadium (IV).

Conclusions

The hydrothermal synthesis of a novel inorganic−organic hybrid vanadium phosphite with the formula (VO)$_4$(4,4′-bpy)$_2$(HPO$_3$)$_4$ and its crystal structure have been described. This structure consists of layers of vanadium(IV) phosphite pillared through 4,4′-bpy ligands into a 3D structure. It is noteworthy that, in Lii and co-workers reported vanadium/phosphate/4,4′-bpy compounds, the valences of the vanadium ions of (4,4′-H$_2$bpy)[V$_2$(HPO$_4$)$_4$(4,4′-bpy)$_2$] (2D), [(VO$_2$)$_2$-(4,4′-bpy)$_{0.5}$(4,4′-Hbpy)(PO$_4$)]·H$_2$O (2D), and (NH$_4$)[(V$_2$O$_3$)$_2$-(4,4′-bpy)$_2$(H$_2$PO$_4$)(PO$_4$)$_2$]·0.5H$_2$O (3D) are +3, +5, and +4/+5 mixed-valence, respectively. However, all of the vanadiums in compound **1** are tetravalent. It is the first member of the vanadium/phosphite/4,4′-bpy system. Compound **1** is thermally stable below 420 °C. Magnetic susceptibility confirms the valence of the vanadium atoms. Clearly, this phosphite as well as other reported inorganic−organic hybrid phosphites to date have shown some distinguished structural features and their own formation mechanisms are different from those for the phosphates. The higher reactivity of the secondary coordination oxygen atoms in the phosphites was observed, and the μ_3-coordination for the phosphites, which is different from the μ_4-coordination for the phosphates, presents further challenges in the formation of a novel family of inorganic−organic hybrid open-framework phosphites.

Acknowledgment. We thank the National Natural Science Foundation of China (Grant No. 20071013), the State Basic Research Project of China (Grant G2000077507), and the Foundation for "Chang-Jiang" scholarship of the Ministry of Education of China for support.

Supporting Information Available: X-ray crystallographic files in CIF format for the structure determination of **1**. This material is available free of charge via the Internet at http://pubs.acs.org.

IC0261676